Available online at www.sciencedirect.com
SCIENCE DIRECT
Journal of Catalysis 238 (2006) 394–401
JOURNAL OF CATALYSIS
www.elsevier.com/locate/jcat

Surface thiolation of carbon nanotubes as supports: A promising route for the high dispersion of Pt nanoparticles for electrocatalysts

Yong-Tae Kim, Tadaoki Mitani *

School of Materials Science, Japan Advanced Institute of Science and Technology, 1-1 Asahidai, Nomi, Ishikawa 923-1292, Japan

Received 12 September 2005; revised 7 December 2005; accepted 16 December 2005

Available online 27 January 2006

Abstract

This paper introduces a unique method for achieving high dispersion of precious metal nanoparticles on carbon nanotube supports for electrocatalysts: the surface thiolation of multiwall carbon nanotubes (MWNT). The high dispersion of Pt nanoparticles [i.e., small average particle size (1.5 nm) and narrow size distribution] was obtained by the surface thiolation of MWNT as supports, despite a considerably large Pt load (40 wt% Pt to MWNT) and the use of MWNT with a relatively small surface area as supports to common activated carbon. In particular, EXAFS and XPS data revealed that the interaction between Pt nanoparticles and surface thiol groups on MWNT was the reason for the high dispersion. These highly dispersed Pt nanoparticles showed enhanced and stable electrocatalytic activity in methanol oxidation and oxygen reduction reactions. This result indicates that the surface thiolation of supports is an effective way to obtain highly dispersed precious metal nanoparticles to enhance electrocatalytic activity.

Keywords: Surface functionalization; Thiol groups; Carbon nanotubes; Pt nanoparticles; High dispersion; Electrocatalyst

1. Introduction

Highly dispersed Pt nanoparticles on carbon supports have been used in a number of heterogeneous catalysis applications, including eletrocatalysts for fuel cells and catalysts for hydrogenation reactions [1,2]. These catalysis reactions occur entirely on the surface of Pt nanoparticles, so high dispersion is required to elevate catalytic activity and reduce the amount of expensive precious metal used. Notably, the high dispersion is more important in electrocatalysts for fuel cells than in catalysts for organic synthesis or environmental purification, because of the large load (about 20–80%) of precious metal required. The wide variety of pore structures and chemical functional groups on the surface of carbon supports affects the dispersion of Pt nanoparticles [3]. For this reason, various high-dispersion studies have been conducted by modifying the pore structure and chemical nature of the carbon supports [4–9]. Among various carbon supports, carbon nanotubes (CNTs) are very attractive as electrocatalyst supports. There has been increased interest in the use of CNTs as supports since the first study on such an application in 1994 [10]. CNTs are adequate as supports for various heterogeneous catalysts, especially electrocatalysts, because they have unique physicochemical characteristics, such as good intrinsic conductivity, a pore structure without micropores, durability under corrosive conditions, and mechanical toughness. However, their inert surface nature [11] due to a perfect graphene sheet structure has hindered the high dispersion of precious metal with uniform size distribution using the conventional impregnation method, in which the affinity of the carbon surface for the precursor solution exerts the dominant effect on dispersion in the deposition step [12]. To solve this problem, the surfaces of CNTs have been functionalized with functional groups like carboxyl [13–15], amine [16], and sulfone [17] groups or polymers [18] having a good affinity with precious metal, using various organic synthetic or electrochemical methods.

In this study, we obtained highly dispersed Pt nanoparticles by introducing thiol groups on multiwall carbon nanotube (MWNT) surfaces, using organic synthetic methods based on an amide bond formation. The thiol groups, well-known func-

* Corresponding author.
E-mail address: mitani@jaist.ac.jp (T. Mitani).

0021-9517/$ – see front matter
doi:10.1016/j.jcat.2005.12.020

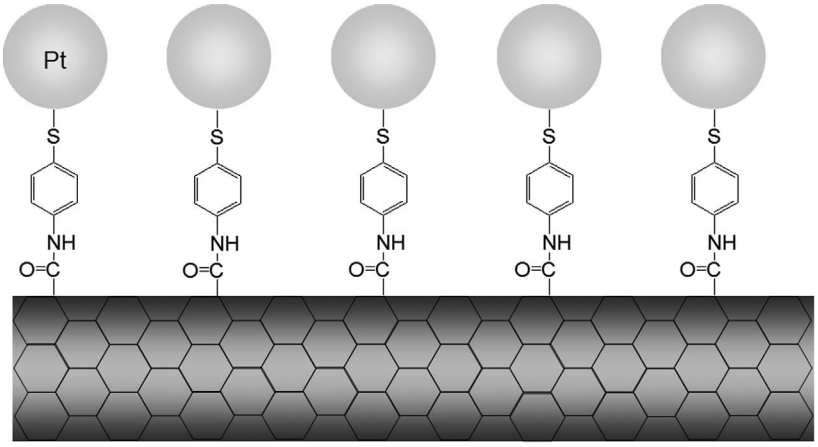

Fig. 1. Schematic illustration of Pt nanoparticles supported on thiolated MWNT.

tional groups forming a spontaneous bond with precious metal surfaces, as in the case of self assembled monolayers (SAMs), were expected to prevent agglomeration among the Pt nanoparticles on MWNTs by a strong interaction with the precious metal (a schematic illustration is presented in Fig. 1).

2. Experimental

2.1. Surface thiolation of MWNTs

MWNTs were prepared by decomposing acetylene on iron nanoparticles supported on silica at 800 °C, which is a slightly modified method of that described previously [19]. This raw soot containing the MWNTs was heated for 2 h at 450 °C in static air and treated for 12 h with 3 M HCl (Kanto Chemical) at 70 °C. Thiolation of MWNTs was conducted by a method based on the formation of an amide bond [20]. Purified MWNTs (p-MWNTs) were stirred in concentrated HNO_3 (70%, Kanto Chemical) for 15 min to prepare carboxylated MWNTs (c-MWNTs), then chlorinated by refluxing for 12 h with $SOCl_2$ (Wako) at 70 °C. After the remaining thionyl chloride was evaporated, the thiolated MWNTs (t-MWNTs) were obtained by reacting with $NH_2C_6H_4SH$ (Wako) in dehydrated toluene (Aldrich) for 24 h at 70 °C.

2.2. Electrocatalyst preparation

To support Pt nanoparticles on the MWNTs, we adopted the well-known impregnation method followed by liquid-phase borohydride. A mixture of 20 mg of various MWNTs (p-, c-, and t-MWNTs) and 6.25 ml of 10 mM H_2PtCl_6 (Aldrich) was suspended by sonication in 40 ml of deionized water. Subsequently, this Pt precursor was reduced and supported on MWNTs simultaneously by $NaBH_4$ (Kanto Chemical) as the reducing agent and washed with deionized water several times. The filtrate was collected to determine an exact load by measuring the Pt residue. After drying, the 40 wt% Pt nanoparticles supported on three kinds of MWNTs – Pt/p-MWNT, Pt/c-MWNT, and Pt/t-MWNT – were obtained. Pt black was also prepared by the same method but without supports.

2.3. Characterization

Fourier transform infrared spectroscopy (FTIR), using a Thermo Nicolet AVATAR 360, was conducted to characterize the carboxylation of the MWNTs. Quantitative assay of the introduced functional groups, especially the carboxyl groups, was done using the Boehm titration method [21]. Titration was conducted in the following order. Oxidized MWNTs (50 mg) were placed in 25 ml of 0.01 M NaOH and suspended in a strong ultrasonic homogenizer for 10 min. This suspension solution was stirred for 24 h at room temperature in a closed vessel and then filtered. Subsequently, 20 ml of this filtrate was reacted with the same amount of 0.01 M HCl for 24 h, and then this solution was back-titrated with 0.01 M NaOH. Oxidized and thiolated MWNTs were subjected to zeta potential measurement (ELS-8000, Otsuka) to evaluate a surface charge. The exact Pt load was determined by inductively coupled plasma atomic emission spectrometry (ICP-AES; Optima 3000DV, Perkin-Elmer). Transmission electron microscopy (TEM; H7100, Hitachi) images were obtained at an accelerating voltage of 100 kV. X-Ray diffractometry (XRD; M18XHF-SRA, MAC Science) analysis was carried out using a Cu-K_α source at room temperature. The average particle size was calculated by the Debye–Scherrer equation using a Pt(111) peak fitted by modified Gaussian function. X-Ray photoelectron spectroscopy (XPS; PHI 5600, ULVAC-PHI) was used to identify the thiolation of the MWNTs and the interaction between the Pt nanoparticles and thiol groups on the MWNTs. Extended X-ray analysis fine structure (EXAFS) data for Pt-L_{III} absorption edges were obtained with transmission mode using the synchrotron radiation of BL01B1, SPring-8, at room temperature. X-Rays were monochromated with two Si(111) planes gratings and detected by two ion chambers, which were continuously purged with a gas mixture of 15% Ar and 85% N_2 in I_0 and 100% Ar gas in I_1. The data reduction was carried out using the ATHENA software. The XANES spectrum was normalized by the Victoreen function, and the radial distribution function (RDF) of EXAFS was obtained by a Fourier transform, in the range of 3–14 $Å^{-1}$ in k space, on k^3-weighted EXAFS oscillations.

2.4. Electrocatalytic activity and stability test

The electrocatalytic activity on methanol oxidation reaction (MOR) or oxygen reduction reaction (ORR) was evaluated by cyclic voltammetry (CV; 608A, ALS). The voltammograms for MOR were recorded at a scan rate of 50 mV s^{-1} from 0 to 960 mV [vs. a saturated calomel electrode (SCE)] in 0.5 M H_2SO_4 + 2 M CH_3OH electrolyte after electrochemical cleaning, which is well-known process for removing the contaminant from an electrode surface by using very fast cycling with 200 mV s^{-1} [22]. An ORR activity test was performed using a rotating disk electrode with a speed of 5000 rpm at a scan rate of 10 mV s^{-1} from 800 to −200 mV (vs. SCE) in 0.1 M $HClO_4$ electrolyte saturated with oxygen after the electrode cleaning. The working electrode was a glassy carbon electrode, 3 mm in diameter, coated with the electrocatalyst layer. Then 3 mg of 40% Pt supported on various MWNTs and 6 μL of ethanol containing 5 wt% Nafion solution were placed in 300 μL of isopropyl alcohol and suspended with sonication for 1 h. A 6-μL portion of this slurry was dropped onto a glassy carbon electrode and dried in a 60 °C oven for 1 h. The counter and reference electrodes were a Pt wire and a SCE, respectively. Electrochemical and thermal stability were tested with CV for MOR and thermogravimetric analysis (TGA; EXSTAR6000, SEIKO), respectively.

3. Results and discussion

3.1. Brief characterization

Before MWNTs are thiolated, carboxylic groups should be introduced on the walls and ends of the MWNTs using various oxidizing agents [20,23–26]. Fig. 2 shows the FTIR spectra of three kinds of MWNTs according to the sequence of surface thiolation. The peak around 1725–1715 cm^{-1}, corresponding to the stretching of C=O in carboxyl groups, drastically increased for c-MWNT, meaning that oxidization with HNO_3 successfully introduced the carboxyl groups on the MWNT surfaces. It is possible to estimate the amount of introduced carboxyl groups using the Boehm titration method [21]; the value obtained for c-MWNT was 2.25 mmol H^+ equiv g^{-1}. After thiolation, the peak decreased, indicating the change of chemical circumstance of C=O in the carboxyl groups due to amide bond formation. Indeed, we tried to assay the thiol groups with FTIR; however, detection proved too difficult because of their weak response in the IR mode. For this reason, we used XPS to directly detect the sulfur atom. The S2p spectra of various MWNTs, given in Fig. 3, show that MWNT thiolation was accomplished. The number of thiol groups and carboxyl groups would be expected to be almost equal, because the amide bond formation via chlorination is a simple reaction exhibiting an almost 100% yield [27].

After Pt loading (40 wt%) on various MWNTs with borohydride reduction, the exact Pt load was determined with ICP-AES. The actual value of the Pt load was 38.8% for Pt/p-MWNT, 39.6% for Pt/c-MWNT, and 39.8% for Pt/t-MWNT, demonstrating that the Pt support was fairly successful. Before providing a detailed discussion of the effect of surface thiol groups on high dispersion, we briefly discuss the characterization of three kinds of Pt/MWNTs with TEM and XRD.

As shown in Fig. 4, the effect of surface thiol groups is clearly seen in the drastically enhanced dispersion for Pt/t-MWNT. The average size of Pt nanoparticles was 4.7 nm on Pt/p-MWNT, 4.2 nm on Pt/c-MWNT, and 1.5 nm on Pt/t-MWNT. The detailed size distribution is presented in Fig. 5. Their average size can also be calculated from the Pt(111) peak of the XRD data presented in Fig. 6 using the Debye–Scherrer equation. Although the sizes of the Pt nanoparticles for Pt/p-MWNT and Pt/c-MWNT could be calculated from the XRD data, it was impossible to determine the particle sizes for Pt/t-MWNT because of their ambiguous peaks, indistinguishable from the background for calculation.

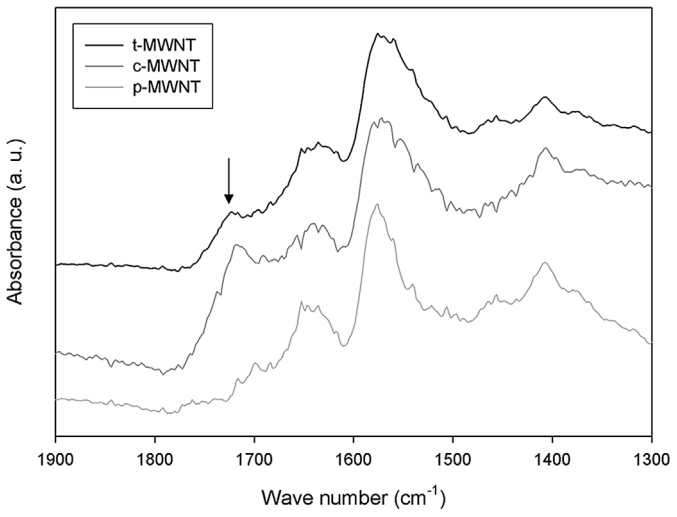

Fig. 2. FTIR spectra of three kinds of MWNT according to the sequence of surface thiolation.

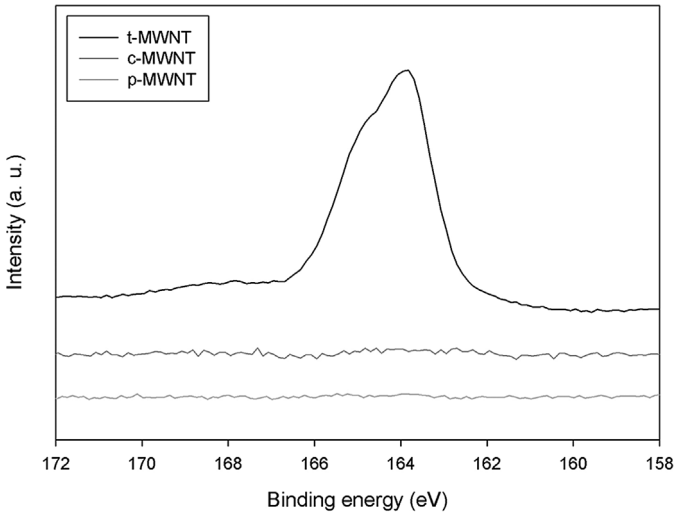

Fig. 3. S2p XPS spectra of three kinds of MWNT calibrated with a value of C1s (284.5 eV) according to the sequence of surface thiolation.

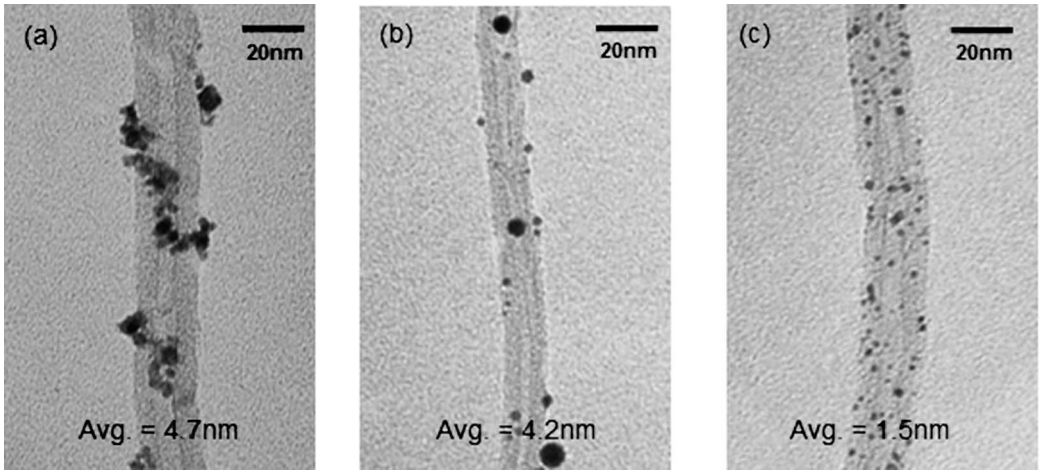

Fig. 4. TEM images of (a) Pt/p-MWNT, (b) Pt/c-MWNT and (c) Pt/t-MWNT obtained with accelerating voltage of 100 kV.

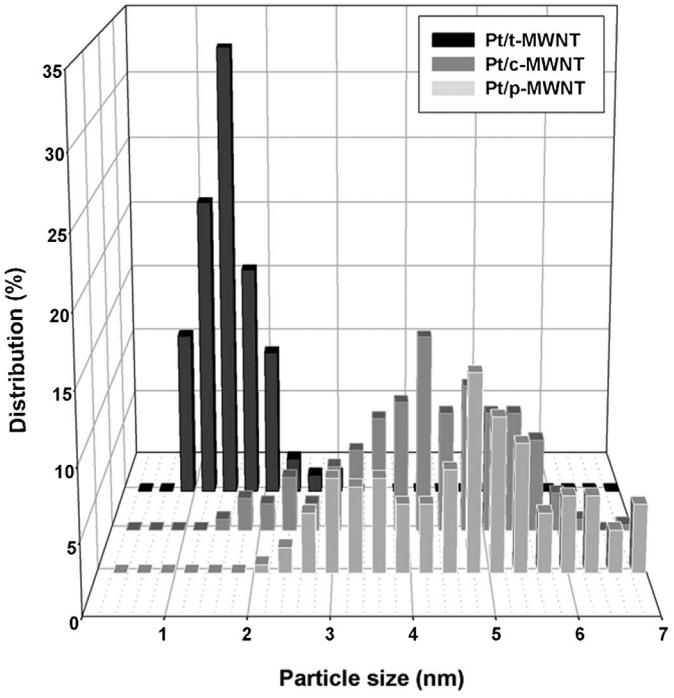

Fig. 5. Size distributions of three kinds of Pt/MWNT. The particle sizes are evaluated from counting and averaging TEM images.

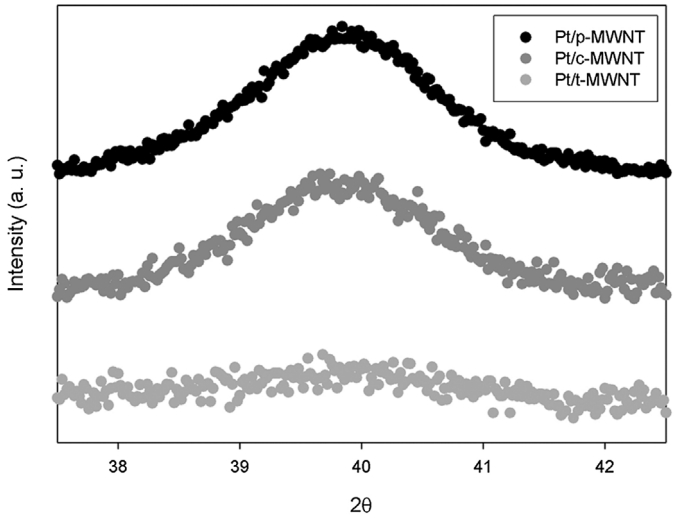

Fig. 6. Detailed patterns of Pt(111) in the powder XRD of three kinds of Pt/MWNT. The particle sizes were calculated from Pt(111) peaks of detailed powder XRD patterns, using the Debye–Scherrer equation.

3.2. *Effect of surface thiol groups on high dispersion*

In general, the surface change of the support is recognized as a very important factor affecting metal dispersion. We measured ζ potential to clarify the effect of surface charge on dispersion. As shown in Fig. 7, the isoelectric point (IEP) was 4.547 for c-MWNT. This result indicates that there is a repulsive force between Pt precursor ions and the surface of c-MWNT (which is very negative) to achieve high dispersion, because the pH of the Pt precursor solution is around 4.0. In contrast, little charge is expected on the surface of p-MWNT or t-MWNT, because they have no functional groups (like carboxyl groups) to generate a surface charge. Although the thiol groups ($pK_a = 8.22$, determined in cysteine [28]) for t-MWNT can also provide a slight surface charge, this pK_a value is negligibly smaller than that of carboxyl groups ($pK_a = 4.74$, determined in acetic acid [29]). Indeed, precisely determining the ζ potential of t-MWNT was almost impossible, because t-MWNT is nondispersible in water.

Fig. 8a shows the XPS survey patterns of samples prepared by simple filtration of the Pt precursor and MWNT mixed solution before $NaBH_4$ reduction. Unexpectedly, there is a clear Pt4f peak at around 73 eV for Pt/t-MWNT, in contrast to no peak for Pt/p-MWNT and Pt/c-MWNT. In view of the surface charge alone, it is natural that Pt cannot be detected for Pt/p-MWNT and Pt/c-MWNT, because there is no electrical interaction between the Pt precursor ions and the surface of MWNT (there is even a repulsive force for Pt/c-MWNT) without any pH adjustment. Similarly, it is not possible to detect Pt in Pt/t-MWNT, because t-MWNT has little surface charge. Hence, this clear Pt4f peak should be assigned to the chemisorption of Pt precursor on surface thiol groups.

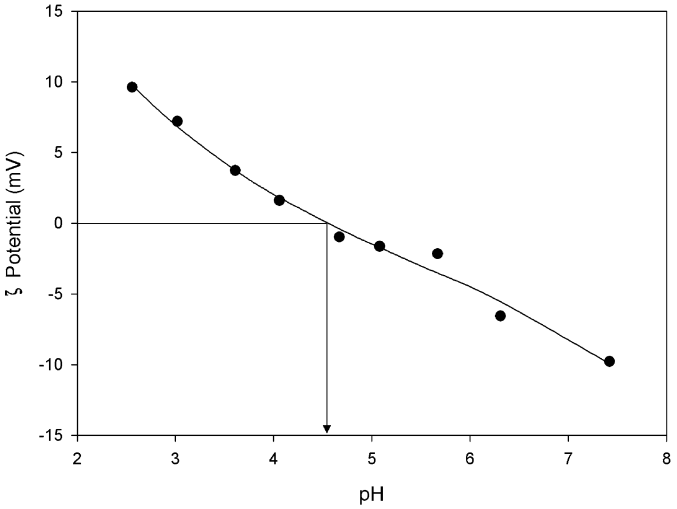

Fig. 7. ζ potential change of c-MWNT as a function of pH.

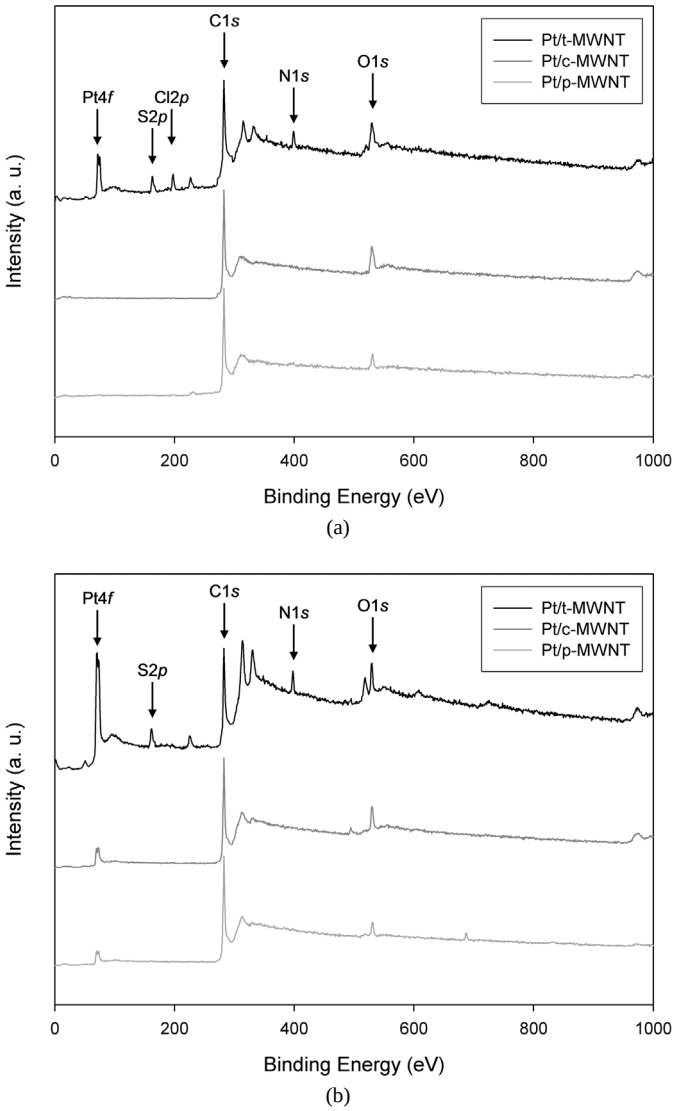

Fig. 8. XPS surveys of various Pt/MWNT (a) before and (b) after borohydride reduction.

Fig. 8b shows the XPS survey patterns of samples after the reduction. On reduction with $NaBH_4$, the Pt4f peak appears in all samples. Notably, a very strong Pt4f peak is seen for Pt/t-MWNT. This indicates that the dispersion of Pt/t-MWNT is much higher than that of the other two samples, because XPS is a surface-sensitive tool. This very high dispersion for Pt/t-MWNT is attributed to the simultaneous initiation of Pt nanoparticle growth from numerous adsorbed Pt precursor ions on surface thiol groups as crystal seeds.

In general, the reaction between metal surface and thiol groups can be written as

$$\mathrm{RSH} + \mathrm{M}_n^0 \rightarrow \mathrm{RS}^-\mathrm{M}^+\mathrm{M}_{n-1}^0 + \tfrac{1}{2}\mathrm{H}_2,$$

which enables the change in the electronic state of metal surfaces and sulfur atoms [30]. It is therefore possible to detect the shift in binding energies with XPS. Fig. 9a shows that the Pt4f

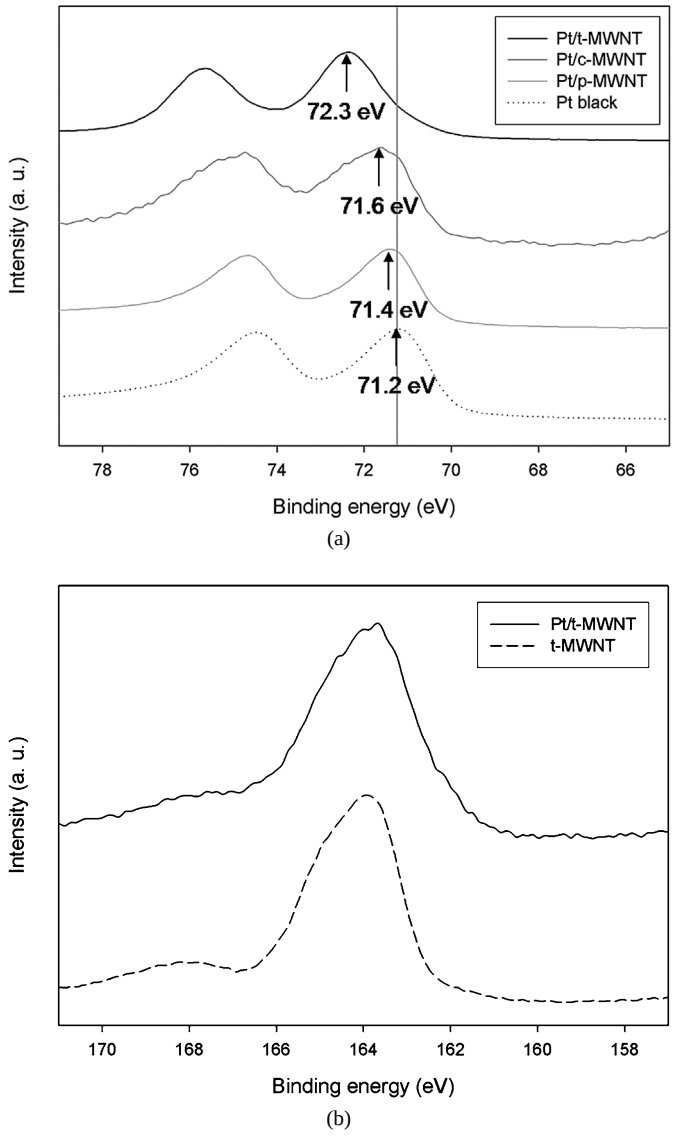

Fig. 9. (a) Pt4f spectra of XPS of three kinds of Pt/MWNT and Pt black. (b) S2p spectra of XPS of thiol groups on MWNT according to the existence of Pt nanoparticles. The XPS spectra were obtained by calibration based on a value of C1s (284.5 eV).

peak of Pt/t-MWNT shifted toward a higher binding energy compared with Pt black, which was assumed to have characteristics similar to bulk Pt. This shift of binding energy is attributable to two main factors: particle size effect and ligand effect. Several studies have investigated the relationship between particle size and binding energy shift; the binding energy is shifted toward higher energy with decreasing particle size, which can be elucidated in terms of final state relaxation [30–32]. The binding energy shift of XPS is also due to the surface ligands of the nanoparticles. Fu et al. demonstrated the ligand effect on the shift using same-sized nanoparticles with various ligands [33]; they claim that around 40% of the binding energy shift was due to the ligand effect. In our study, the binding energy of Pt/t-MWNT shifted by 1.1 eV from that of Pt black. This fairly large shift is attributable to both the size and the ligand effect, that is, the decreased nanoparticle size (1.5 nm) and the interaction between Pt nanoparticles and thiol groups on MWNTs. The shift in the S2p peak has been reported in many studies of SAMs, and it is well known that the S2p peak is shifted toward low binding energy by adsorption on a gold or platinum substrate [34,35]. The shift in the S2p peak of Pt/t-MWNT (Fig. 9b) toward low binding energy compared with t-MWNT in the present study is consistent with previous reports.

Direct evidence of the effect of surface thiol groups on Pt/t-MWNT dispersion was obtained from the RDF of the Fourier-transformed EXAFS. As shown in Fig. 10, for Pt/t-MWNT, the peak around $R = 1.9$ Å, corresponding to 1NN of Pt–S, clearly shows the existence of Pt–S bonding, whereas no such peak is seen for Pt/p-MWNT or Pt/c-MWNT. Moreover, a smaller peak of Pt/t-MWNT than of other samples around $R = 2.7$ Å, corresponding to 1NN of Pt–Pt, can be explained by the decreased coordination number with increasing particle size. Hence, the high Pt/t-MWNT dispersion is attributed to the effect of surface thiol groups as anchorage centers, which protect against an agglomeration among Pt nanoparticles by Pt–S bond formation, demonstrating that the suggested model in Fig. 1 is reasonable.

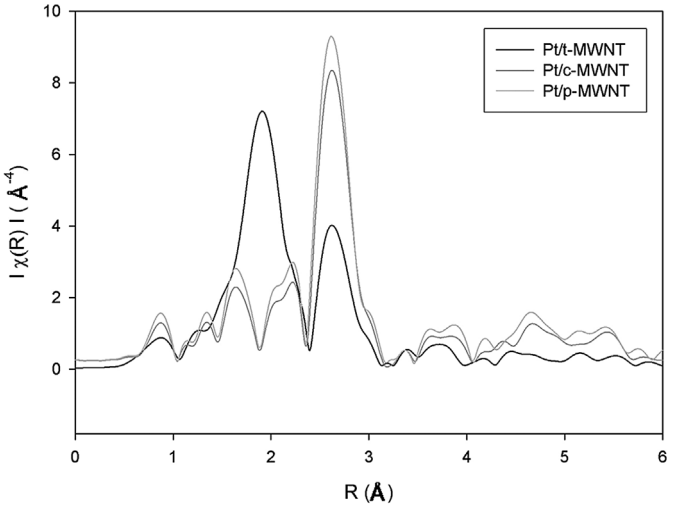

Fig. 10. RDF of EXAFS as the direct evidence of the effect of surface thiol groups on high dispersion for Pt/t-MWNT.

3.3. Electrocatalytic activity for MOR and ORR

To investigate the relationship between dispersion and electrocatalytic activity, we carried out CV measurements on the MOR (Fig. 11) and ORR (Fig. 12) with three kinds of prepared Pt/MWNT and a commercial electrocatalyst (E-TEK, 40 wt% Pt/Vulcan XC72) as a reference. Figs. 11 and 12 clearly show that with decreasing Pt particle size, electrocatalytic activity increases noticeably for MOR and slightly for ORR. This enhanced activity of Pt/t-MWNT for MOR is attributed to the increased surface area created by high dispersion. Moreover, surface thiol groups are considered to have little effect on the electron transfer from Pt nanoparticles to MWNTs as insulators or tunneling barriers. In contrast, the slight increase of ORR activity for Pt/t-MWNT can be elucidated by the fact that there is an optimum particle size of electrocatalyst for ORR (about 3 nm). This is because the specific activity per Pt surface area tends to increase with increasing particle size, although larger particles have smaller active surface areas for

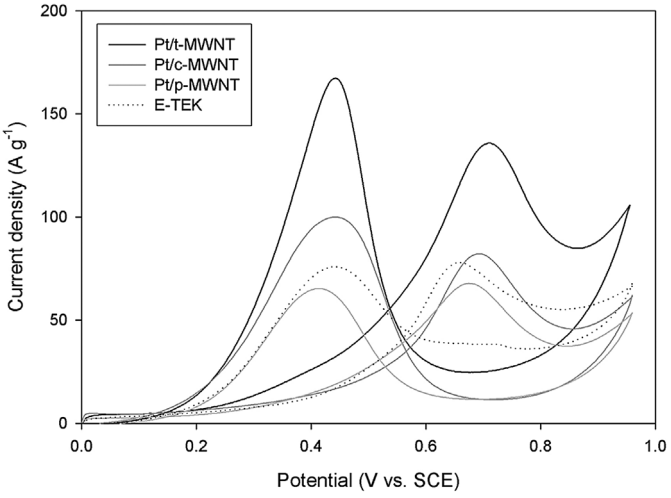

Fig. 11. CV curves on methanol oxidation reaction of three kinds of Pt/MWNT and commercial samples.

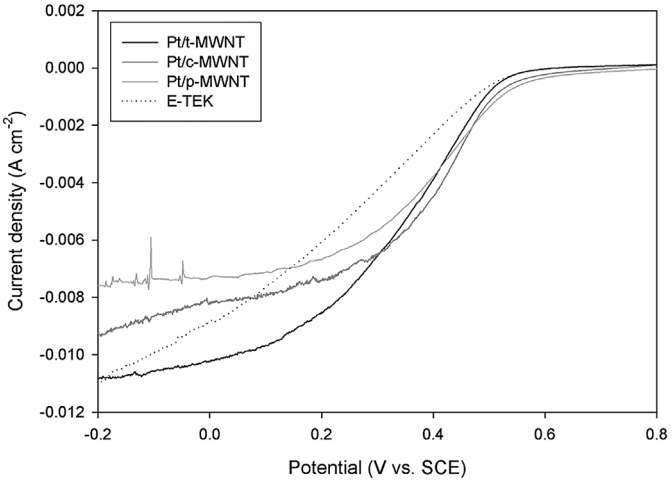

Fig. 12. CV curves on oxygen reduction reaction of three kinds of Pt/MWNT and commercial samples.

ORR [36,37]. Compared with the commercial electrocatalyst, 40% Pt/Vulcan XC72 with an average particle size of around 2.8 nm determined by E-TEK, Pt/t-MWNT showed enhanced activity for both MOR and ORR, whereas Pt/c-MWNT and Pt/MWNT showed similar or less activity due to relatively low dispersion. Especially in the case of ORR, Pt/t-MWNT showed a steeper increase in reduction current than the E-TEK samples, even though the maximum currents are similar. This result is attributable to the superior intrinsic conductivity of CNTs over Vulcan XC72 as a support, indicating the increasing operational voltage of the fuel cell. Although sulfur is generally recognized to be a surface poison that decreases electrocatalytic activity, no such effect of the sulfur of thiol groups was shown for Pt/t-MWNT in both MOR and ORR. This is because the sulfur is adsorbed at a part of the Pt surfaces as an anchorage center rather than over the entire surface, as shown in Fig. 1. These results indicate that the introduction of surface thiol groups is an especially effective method for electrocatalyst, which require a large load of precious metal nanoparticles on the highly crystallized carbon materials, like CNTs, which have relatively small surface areas.

3.4. Electrochemical and thermal stability of Pt/t-MWNT

Electrochemical and thermal stability, very important factors in the application to practical fuel cells, were tested using long-term CV (Fig. 13) for MOR and TGA (Fig. 14) under air flow. As Fig. 13 shows, electrochemical stability for Pt/t-MWNT is fairly good, similar to that of the other samples, indicating that the surface thiol groups as linkers are stable in this condition. The slight decrease after about 350 cycles is attributable to gradual surface poisoning by CO and the decrease of methanol as a reactant. The TGA results in Fig. 14 show that Pt/t-MWNT was thermally stable by about 600 K, but the surface thiol groups decomposed rapidly from about 600 K (the first peak in DTG) and the CNTs decomposed from about 700 K (the second large peak in DTG). This means that the current Pt/t-MWNT is suitable as a electrocatalyst only in low-temperature fuel cells, such as polymer electrolyte membrane fuel cells and direct methanol fuel cells. Nonetheless, we believe that this limit of stability can be improved by changing the surface thiol groups to those with a more thermally stable backbone or by devising a new route for surface thiolation.

4. Conclusion

This study investigated a new approach to achieving highly dispersed metal nanoparticles by thiolating the supports. The thiolation of MWNTs was conducted by organic synthesis, and the Pt nanoparticles were supported with an impregnation method followed by a liquid-phase borohydride reduction. Subsequently, the characterization of Pt nanoparticles on thiolated MWNTs was done with several analysis techniques, including TEM, XRD, XPS, and EXAFS. This surface thiolation method enabled us to obtain a high dispersion of Pt nanoparticles, even when a large metal load was required on the supports with small surface areas, as in the case of electrocatalysts for fuel cells.

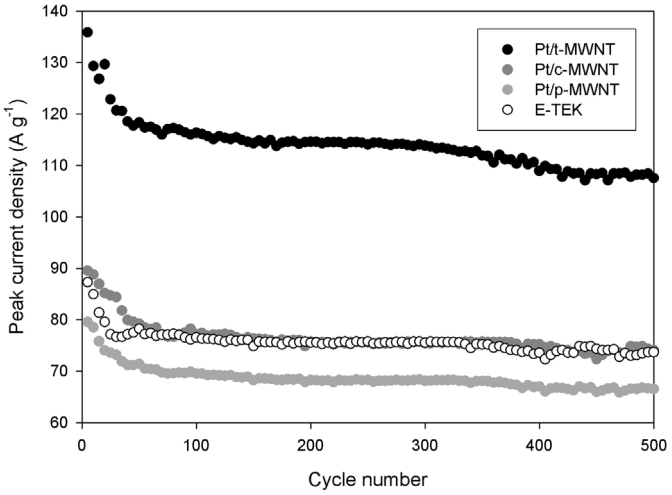

Fig. 13. Electrochemical stability test with long-term CV in MOR. Current densities are based on geometric surface area.

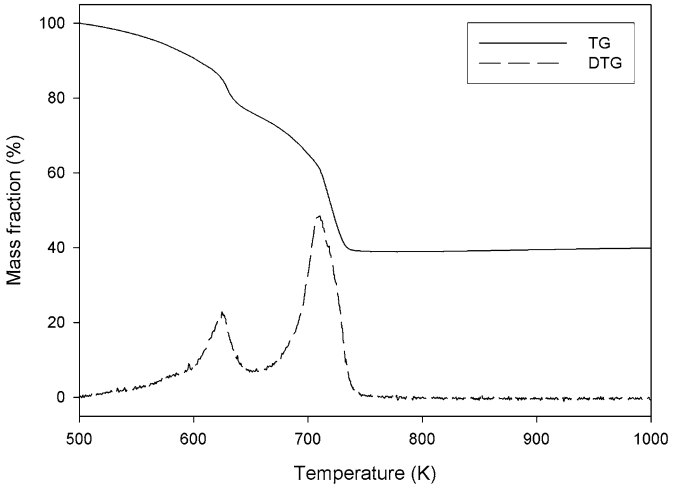

Fig. 14. Thermal stability test with TGA under air flow.

This result can be attributed to the simultaneous initiation of Pt nanoparticle growth from numerous adsorbed Pt precursor ions on the surface thiol groups as crystal seeds. The enhanced dispersion of Pt nanoparticles provided a higher electrocatalytic activity in both MOR and ORR, and the particles were electrochemically stable in MOR and thermally stable below 600 K. Finally, the thiolation of supports is an effective method of achieving a high dispersion of precious metal nanoparticles and can be applied to the preparation of various catalysts and electrocatalysts.

Acknowledgments

This work was partly supported by the Japanese Ministry of Education, Science, Sports, and Culture through a Grant-in-Aid for Scientific Research (B) (17310059) and the Nanotechnology Support Project (proposal 2005A0702-NXa-np/BL01B1), with the approval of the Japan Synchrotron Radiation Research Institute (JASRI). The authors thank Dr. Takashi Okubo of Northwestern University for his kind help with the XPS mea-

surements, and Atsushi Yamashita and Yoon Ki Jung of JAIST for their assistance with the ζ potential measurements.

References

[1] A. Wieckowski, E.R. Savinova, C.G. Vayenas, Catalysis and Electrocatalysis at Nanoparticle Surface, Marcel Dekker, New York, 2003.
[2] S. Nishimura, Handbook of Heterogenous Catalytic Hydrogenation for Organic Synthesis, John Wiley & Sons, New York, 2001.
[3] K. Kinoshita, Carbon: Electrochemical and Physicochemical Properties, Wiley, New York, 1988.
[4] P. Ehrburger, P.L. Walker, J. Catal. 55 (1978) 63.
[5] A. Linares-Solano, F. Rodriguez-Reinoso, C.S.-M.d. Lecea, O.P. Mahajan, P.L. Walker, Carbon 20 (1982) 177.
[6] C. Prado-Burguete, A. Linares-Solano, F. Rodriguez-Reinoso, C.S.-M.d. Lecea, J. Catal. 115 (1989) 98.
[7] G. De la Puente, A. Centeno, A. Gil, P. Grange, J. Colloid Interface Sci. 202 (1998) 155.
[8] S.H. Joo, S.J. Choi, I. Oh, J. Kwak, Z. Liu, O. Terasaki, R. Ryoo, Nature 412 (2001) 169.
[9] T. Yoshitake, Y. Shimakawa, S. Kuroshima, H. Kimura, T. Ichihashi, Y. Kubo, D. Kasuya, K. Takahashi, F. Kokai, M. Yudasaka, S. Iijima, Physica B 323 (2002) 124.
[10] J.M. Planeix, N. Coustel, B. Coq, V. Brotons, P.S. Kumbhar, R. Dutartre, P. Geneste, P. Bernier, P.M. Ajayan, J. Am. Chem. Soc. 116 (1994) 7935.
[11] E. Dujardin, T.W. Ebbesen, H. Hiura, K. Tanigaki, Science 265 (1994) 1850.
[12] K. Kinoshita, P. Stonehart, in: J.O.M. Bockris, B.E. Conway (Eds.), Modern Aspects of Electrochemistry, Plenum, New York, 1977.
[13] V. Lordi, N. Yao, J. Wei, Chem. Mater. 13 (2001) 733.
[14] Z. Liu, X. Lin, J.Y. Lee, W. Zhang, M. Han, L.M. Gan, Langmuir 18 (2002) 4054.
[15] K.I. Han, J.S. Lee, S.O. Park, S.W. Lee, Y.W. Park, H. Kim, Electrochim. Acta 50 (2004) 791.
[16] D.-J. Guo, H.-L. Li, Electroanalysis 17 (2005) 869.
[17] X. Sun, R. Li, D. Villers, J.P. Dodelet, S. Desilets, Chem. Phys. Lett. 379 (2003) 99.
[18] K. Jiang, A. Eitan, L.S. Schadler, P.M. Ajayan, R.W. Siegel, N. Grobert, M. Mayne, M. Reyes-Reyes, H. Terrones, M. Terrones, Nano Lett. 3 (2003) 275.
[19] K. Hernadi, A. Fonseca, J.B. Nagy, D. Bernaerts, A.A. Lucas, Carbon 34 (1996) 1249.
[20] J. Liu, A.G. Rinzler, H. Dai, J.H. Hafner, R.K. Bradley, P.J. Boul, A. Lu, T. Iverson, K. Shelimov, C.B. Huffman, F. Rodriguez-Macias, Y.-S. Shon, T.R. Lee, D.T. Colbert, R.E. Smalley, Science 280 (1998) 1253.
[21] H.P. Boehm, E. Diehl, W. Heck, R. Sappok, Angew. Chem. 76 (1964) 742.
[22] H.-J. Kim, K.-S. Yun, E. Yoon, J. Kwak, Electrochim. Acta 50 (2004) 205.
[23] D.B. Mawhinney, V. Naumenko, A. Kuznetsova, J.T. Yates Jr., J. Liu, R.E. Smalley, J. Am. Chem. Soc. 122 (2000) 2383.
[24] D.B. Mawhinney, V. Naumenko, A. Kuznetsova, J.T. Yates, J. Liu, R.E. Smalley, Chem. Phys. Lett. 324 (2000) 213.
[25] T. Kyotani, S. Nakazaki, W.-H. Xu, A. Tomita, Carbon 39 (2001) 782.
[26] J. Zhang, H. Zou, Q. Quan, Y. Yang, Q. Li, Z. Liu, X. Guo, Z. Du, J. Phys. Chem. B 107 (2003) 3712.
[27] V. Maurizot, C. Dolain, I. Huc, Eur. J. Org. Chem. 7 (2005) 1293.
[28] S.G. Tajc, B.S. Tolbert, R. Basavappa, B.L. Miller, J. Am. Chem. Soc. 126 (2004) 10508.
[29] D.R. Lide, CRC Handbook of Chemistry and Physics, 76th ed., CRC Press, New York, 1995.
[30] G.K. Wertheim, S.B. Dicenzo, S.E. Young, Phys. Rev. Lett. 51 (1983) 2310.
[31] W. Eberhardt, P. Fayet, D.M. Cox, Z. Fu, A. Kaldor, R. Sherwood, D. Sondericker, Phys. Rev. Lett. 64 (1990) 780.
[32] T.T.P. Cheung, Surf. Sci. 140 (1984) 151.
[33] X. Fu, Y. Wang, N. Wu, L. Gui, Y. Tang, J. Colloid Interface Sci. 243 (2001) 326.
[34] R.G. Nuzzo, B.R. Zegarski, L.H. Dubois, J. Am. Chem. Soc. 109 (1987) 733.
[35] D.G. Castner, K. Hinds, D.W. Grainger, Langmuir 12 (1996) 5083.
[36] K. Kinoshita, J. Electrochem. Soc. 137 (1990) 845.
[37] N. Giordano, E. Passalacqua, L. Pino, A.S. Arico, V. Antonucci, M. Vivaldi, K. Kinoshita, Electrochim. Acta 36 (1991) 1979.